V European Conference on Computational Fluid Dynamics
ECCOMAS CFD 2010
J. C. F. Pereira and A. Sequeira (Eds)
Lisbon, Portugal,14-17 June 2010

INTERNAL TURBULENT TWO-PHASE FLOWS FORMED BY WALL INJECTION OF FLUID AND PARTICLES

Konstantin N. Volkov*

*Faculty of Engineering, Kingston University,
Friars Avenue, Roehampton Vale, London, SW15 3DW, United Kingdom
e-mail: k.volkov@kingston.ac.uk

Key words: Gas-Particle Flow, Internal Flow, Turbulence, Large-Eddy Simulation

Abstract. *Simulation of turbulent gas-particle flows inside combustion chambers of energy systems is performed. An advanced model of turbulent particulate flow, which includes effects of particle stochastic motion (particle dispersion) is developed. Numerical calculations are performed by the Eulerian–Lagrangian approach for the fluid and particles. Fluid flow calculations are based on Reynolds-averaged (RANS) or filtered Navier–Stokes (LES) equations. The solid phase is treated by the Lagrangian approach, which means that particles are followed in time along their trajectories through the flow field. At every given time step, the new position of the particle and its new velocity are calculated according to the forces acting on the particle. The inclusion of particle combustion and particle stochastic evolution in modeling of particle dynamics allows the proposed model to realistically simulate the flow field inside a combustion chamber. Substantial knowledge was obtained about particles dynamics as well as their interactions with internal turbulent flow. The two-phase model developed reasonably explains computational and experimental data, in particular, it explains the formation of regions of irregular particles concentration in internal duct flow induced by wall injection of fluid and particles.*

1 INTRODUCTION

Aluminized propellants are used in solid rocket motors to increase specific impulse. Aluminum particles burn in a significant portion of the chamber and produce a condensed phase that is carried out into the flowfield. Aluminum particles affect appreciably combustion instabilities by acting as driving or, on the contrary, as damping mechanisms. Therefore, a reliable stability prediction includes the description of the reactive turbulent two-phase flow in the motor.

The flow in the channel with distributed fluid injection serves as a model for flow of products of solid fuel decomposition in the solid rocket motors, which reflects the essential side of the process — injection of the mass from the burning surface [1–6].

The study focuses on the numerical analysis of turbulent gas-particle flows inside combustion chambers of energy systems. The objective of the study is to develop an advanced model of turbulent particulate flow, which includes effects of particle combustion and particle stochastic motion (particle dispersion). The inclusion of particle combustion and particle stochastic evolution in modeling of particle dynamics allows the proposed model to realistically simulate the flow field inside a combustion chamber.

To describe gas-particle flows, the following approaches are used: kinetic, continual (Eulerian), and trajectory (Lagrangian). Practical realization is dictated by the range of applicability and the possibility of predicting various characteristics of the flow [7–10]. The kinetic approach finds application in works considering the construction and substantiation of mathematical models of gas-particle flows. In solving specific problems, kinetic models are used comparatively rarely because of their complexity. In Eulerian approach, particles are represented in the form of a continuous medium with a continuously space distributed density. The behavior of a multi-velocity continuum is described by the equations in Eulerian coordinates. Modeling of turbulent flows requires the solution of problems related to determination of the degree of involvement of particles in the fluid motion and description of the reverse effect of particles on turbulence. In Lagrangian approach, the equations describing the motion of particles are written in Lagrangian coordinates, and are integrated along the trajectories of sample particles in the fluid field.

Depending on whether or not the influence of velocity fluctuations of the fluid flow on the particle motion is taken into account, one distinguishes two variants of the trajectory approach [7]. In the deterministic model, the interaction of discrete inclusions with turbulent moles is ignored. The position of the sample particle at the initial time completely determines its further evolution. In flows with a large curvature of streamlines, melting and burning of particles, the model leads to errors in determining the characteristics of the two-phase flow. The stochastic model takes into account the influence of turbulence by introducing a random force into the equation of particle motion. The instantaneous velocity of the turbulent flow is a sum of the averaged and random components. The mean component is found from the RANS equations, DNS or LES. The random component is determined by the Monte Carlo method.

The stochastic models described in the literature [9,11–22] are distinguished by physical factors that are taken into account and peculiarities of generating turbulent fluctuations of the fluid flow. In another approach, the calculation of the fluctuation velocity component is based on the integration of a Langevin-type equation [15, 23–35].

Particle turbulent dispersion due to interaction between particles and turbulent eddies of fluid flow is generally dealt with by two methods. The first method, mean diffusion, characterizes only the overall mean (time-averaged) dispersion of particles caused by the mean statistical properties of the turbulence. The second method, structural dispersion, includes the detail of the non-uniform particle concentration structures generated by local instantaneous features of the flow, primarily caused by the spatial-temporal turbulent eddies and their evolution.

Numerical calculations are performed by the Eulerian–Lagrangian approach for the fluid and particles. Fluid flow calculations are based on Reynolds-averaged (RANS) or filtered Navier–Stokes (LES) equations. The solid phase is treated by the Lagrangian approach, which means that particles are followed in time along their trajectories through the flow field. At every given time step, the new position of the particle and its new velocity are calculated according to the forces acting on the particle.

Substantial knowledge was obtained about particle dynamics as well as their interactions with internal turbulent flow. The two-phase model developed reasonably explains computational and experimental data. In particular, it explains the formation of regions of irregular particles concentration in internal duct flow induced by wall injection.

2 FLUID FLOW FIELD

Let us align the x-axis of the Cartesian frame of reference with the lower wall of the channel, and the y- and z-axes with its cross-section. The injection velocities on the lower and upper walls are v_{w1} and v_{w2}.

In Cartesian coordinates (x, y, z), an unsteady 3D flow of a viscous compressible fluid is described by the following equation

$$\frac{\partial Q}{\partial t} + \frac{\partial F_x}{\partial x} + \frac{\partial F_y}{\partial y} + \frac{\partial F_z}{\partial z} = H. \tag{1}$$

Equation (1) is complemented with the equation of state for perfect gas

$$p = (\gamma - 1)\rho \left[e - \frac{1}{2} \left(v_x^2 + v_y^2 + v_z^2 \right) \right].$$

The vector of conservative variables, Q, and the flux vectors F_x, F_y and F_z have the

following form

$$Q = \begin{pmatrix} \rho \\ \rho v_x \\ \rho v_y \\ \rho v_z \\ \rho e \end{pmatrix}, \quad F_x = \begin{pmatrix} \rho v_x \\ \rho v_x v_x + p - \tau_{xx} \\ \rho v_x v_y - \tau_{xy} \\ \rho v_x v_z - \tau_{xz} \\ (\rho e + p) v_x - v_x \tau_{xx} - v_y \tau_{xy} - v_z \tau_{xz} + q_x \end{pmatrix},$$

$$F_y = \begin{pmatrix} \rho v_y \\ \rho v_y v_x - \tau_{yx} \\ \rho v_y v_y + p - \tau_{yy} \\ \rho v_y v_z - \tau_{yz} \\ (\rho e + p) v_y - v_x \tau_{yx} - v_y \tau_{yy} - v_z \tau_{yz} + q_y \end{pmatrix},$$

$$F_z = \begin{pmatrix} \rho v_z \\ \rho v_z v_x - \tau_{zx} \\ \rho v_z v_y - \tau_{zy} \\ \rho v_z v_z + p - \tau_{zz} \\ (\rho e + p) v_z - v_x \tau_{zx} - v_y \tau_{zy} - v_z \tau_{zz} + q_z \end{pmatrix}.$$

The viscous stress tensor, τ_{ij}, and heat flux, q_j, are found from the relations

$$\tau_{ij} = \mu_{\text{eff}} \left(\frac{\partial v_i}{\partial x_j} + \frac{\partial v_j}{\partial x_i} - \frac{2}{3} \frac{\partial v_k}{\partial x_k} \delta_{ij} \right), \quad q_i = -\lambda_{\text{eff}} \frac{\partial T}{\partial x_i}.$$

Here, t is the time, ρ is the density, v_x, v_y, and v_z are the velocity components in the coordinate directions x, y and z, p is the pressure, e is the total energy per unit mass, T is the temperature, and γ is the specific heat ratio.

The equation (1) is suitable for both laminar and turbulent flows, and it formally coincides with unsteady RANS. The effective viscosity, μ_{eff}, is calculated as the sum of molecular viscosity, μ, and eddy viscosity, μ_{sgs}, and the effective thermal conductivity, λ_{eff}, is expressed in terms of effective viscosity and Prandtl number

$$\mu_{\text{eff}} = \mu + \mu_{\text{sgs}}, \quad \lambda_{\text{eff}} = c_p \left(\frac{\mu}{\text{Pr}} + \frac{\mu_{\text{sgs}}}{\text{Pr}_{\text{sgs}}} \right),$$

where c_p is the specific heat capacity at constant pressure, and $\text{Pr} = 0.72$ and $\text{Pr}_{\text{sgs}} = 0.9$.

In the RNG model, the calculation of effective viscosity reduces to the solution of nonlinear equation [36]

$$\mu_{\text{eff}} = \mu \Big[1 + H(X - C) \Big]^{1/3}, \quad X = \frac{\mu_{\text{sgs}}^2 \mu_{\text{eff}}}{\mu^3}, \tag{2}$$

where $H(X)$ is the Heaviside function, and $C = 100$. The eddy viscosity is

$$\mu_{\text{sgs}} = \rho\,(C_R\Delta)\,|S|^2, \quad |S| = (2S_{ij}S_{ij})^{1/2}, \quad S_{ij} = \frac{1}{2}\left(\frac{\partial v_i}{\partial x_j} + \frac{\partial v_j}{\partial x_i}\right), \tag{3}$$

where $C_R = 0.157$. At $X \ll C$, the equation (3) yields the Smagorinsky model [37], and $C_S(2C_R)^{1/4}/2\pi = 0.119$.

To incorporate the effects of curvature of streamlines, the eddy viscosity is multiplied by the damping function depending on the Richardson number [38]. The RNG model is simple and efficient, and correctly predicts the eddy viscosity in the laminar region.

The filter width, Δ, is related to the mesh step size

$$\Delta = V^{1/3} = (\Delta x \Delta y \Delta z)^{1/3},$$

where V is the volume of cell, and Δx, Δy and Δz are mesh steps in the coordinate directions x, y and z.

The normal fluid velocity and wall temperature are specified on lower and upper walls ($v_x = v_z = 0$, $v_y = v_{w1}$, $T = T_{w1}$ at $y = 0$, and $v_x = v_z = 0$, $v_y = -v_{w2}$, $T = T_{w2}$ at $y = h$). Injection velocity is constant in space, and changes in time according to Gaussian law with imposed random fluctuations in the form of white noise [3]. No-slip and adiabatic boundary conditions are used on the left boundary ($v_x = v_y = v_z = 0$, $\partial T/\partial n = 0$ at $x = 0$). Non-reflecting boundary conditions are applied to the outlet boundary of the channel at $x = L$. Periodic boundary conditions are specified in z direction.

3 DISPERSED PHASE

The equations of the translational motion of a spherical particle are written in the form

$$\frac{d\boldsymbol{r}_{\text{p}}}{dt} = \boldsymbol{v}_{\text{p}}, \quad \frac{d\boldsymbol{v}_{\text{p}}}{dt} = \frac{3C_{\text{D}}\rho}{8\rho_{\text{p}}r_{\text{p}}}\,|\boldsymbol{v} - \boldsymbol{v}_{\text{p}}|\,(\boldsymbol{v} - \boldsymbol{v}_{\text{p}})\,. \tag{4}$$

To calculate the drag coefficient, the modified Stokes law is used

$$C_{\text{D}} = \frac{24}{\text{Re}_{\text{p}}} f_{\text{D}}(\text{Re}_{\text{p}}).$$

The function f_{D} takes into account the correction to the Stokes law for the particle inertia, and the relative Reynolds number is

$$\text{Re}_{\text{p}} = \frac{2r_{\text{p}}\rho\,|\boldsymbol{v} - \boldsymbol{v}_{\text{p}}|}{\mu}.$$

The particle relaxation time is calculated by the relation

$$\tau_{\text{p}} = \frac{8\rho_{\text{p}}r_{\text{p}}}{3\rho C_{\text{D}}\,|\boldsymbol{v} - \boldsymbol{v}_{\text{p}}|}.$$

Equations (4) are integrated along the path of an individual particle and require specification of only the initial conditions — the coordinates and velocity at the time $t = 0$. The fluid velocity in equation (4) represents a random function of the spatial coordinates and time. The turbulence is taken into account by introducing random velocity fluctuations into equation (4). The fluid velocity is a sum of the averaged velocity, $\langle \boldsymbol{v} \rangle$, and the random velocity, $\boldsymbol{v}'$. The averaged velocity is precalculated. In order to calculate the random velocity, an eddy lifetime model and a Langevin-type equation are used.

4 EDDY LIFETIME MODEL

The turbulence field is simulated by a set of spherical eddies, each of which is characterized by some velocity v_e, radius L_e and lifetime T_e. In the simplest case, the characteristics of turbulent eddies are assumed to be constant throughout the flow field [11]. In the model of [12], the eddy velocity is considered to be a random, $\boldsymbol{v}_\mathrm{e} = \{u_\mathrm{e}, v_\mathrm{e}, w_\mathrm{e}\}$. The eddy radius and eddy lifetime are determined from the local characteristics of the turbulent flow

$$L_\mathrm{e} = c_\mu^{3/4} \frac{k^{3/2}}{\varepsilon}, \quad T_\mathrm{e} = \frac{L_\mathrm{e}}{(2k/3)^{1/2}},$$

where $c_\mu \sim 0.9$. It is assumed that during the lifetime of the eddy, its velocity and radius remain unchanged. Thus, the turbulent mole loses and acquires its individuality stepwise, which leads to the appearance of turbulent flow fluctuations.

In the model of [14], the eddy lifetime is considered to be a random quantity and is chosen from the Poisson distribution.

Let at some point of the flow a fluid mole (a fluid volume, whose size is characterized by an integral scale of turbulence) be formed. When moving, the fluid mole entrains particles that have gotten into it. The friction between the fluid and the particles retards the mole, and the particles are accelerated. The mole retains its velocity throughout eddy lifetime (from the moment it was released from one layer of the flow until it mixed with another layer). The mole loses its individuality stepwise.

Suppose that at time t_i a particle having velocity $\boldsymbol{v}_\mathrm{p}$ is in the center of a eddy moving with velocity $\boldsymbol{v}_\mathrm{e}$. Taking into account the relative motion of the eddy and the particle at time t_{i+1}, the following three situations are possible: the particle remains within the initial turbulent mole and is moving together with it ($r < L_\mathrm{e}$, case 1), the particle leaves the initial mole ($r < L_\mathrm{e}$, case 2), the lifetime of the eddy expires and it loses its individuality, and the particle thereby gets into a new turbulent mole and begins a new process of interaction ($t_{i+1} - t_i > T_\mathrm{e}$, case 3). In the case 1, in accordance with the new position of the particle and the local characteristics of the turbulence, the new values of the characteristic eddy scales (velocity, radius and lifetime) are calculated (Figure 1). In the cases 2 and 3, the particle gets into a new turbulent mole with different characteristics. The new fluctuation of the fluid flow velocity is determined.

The time in which the particle manages to leave the initial mole is estimated from the

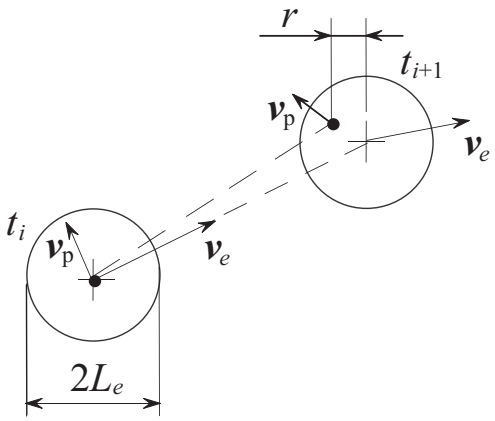

Figure 1: Particle and eddy interaction

linearized equation of motion of the particle

$$T_\mathrm{c} = -\tau_\mathrm{p} \ln\left(1 - \frac{L_\mathrm{e}}{\tau_\mathrm{p}\left|\boldsymbol{v} - \boldsymbol{v}_\mathrm{p}\right|}\right).$$

If $L_\mathrm{e} > \tau_\mathrm{p}\left|\boldsymbol{v} - \boldsymbol{v}_\mathrm{p}\right|$, then the expression for T_c loses meaning. This means that the particle does not leave the eddy and remains in as long as it exists. Hence, as a time criterion for the generation of a new fluctuation, the minimum of the eddy lifetime, T_e, and the time in which the particle passes through the eddy, T_c, is used

$$T = \begin{cases} \min\left(T_\mathrm{e},\, T_\mathrm{c}\right) & \text{if } L_\mathrm{e} > \tau_\mathrm{p}\left|\boldsymbol{v} - \boldsymbol{v}_\mathrm{p}\right|, \\ T_\mathrm{e} & \text{if } L_\mathrm{e} \leqslant \tau_\mathrm{p}\left|\boldsymbol{v} - \boldsymbol{v}_\mathrm{p}\right|. \end{cases}$$

The model of [20] assumes that the particle does not leave the initial mole, which leads to overestimated dispersion of particles. Account of the relative motion of the particle and eddy leads to better agreement between theoretical and experimental data [8, 22].

The time and space criteria for the generation of a random fluid velocity for different models are given in the Table 1.

In the model of [11], the integration step is assumed to be equal to T_e. Such an approach means that as long as it lives the mole interacts with the same particles (particles do not enter the mole and do not leave it). This holds only for averaged-motion equilibrium turbulent flows. If the mean phase velocities differ, the particles pierce the mole and, in so doing, because of their interaction, their velocities are not equal at the entrance to the mole and at the exit from it. As a result, the particles either carry away with them part of the moles momentum or transfer to the mole part of their momentum.

Extension of the model of [11] to more complicated cases requires taking into account the relative motion of the particle and the mole.

In the model of [13], the integration step is chosen so that the particle crosses no more than one cell of the computational mesh. Such an approach, however, is computational

rather than reflecting actual processes. The ideas proposed in [12] proved to be more advanced, and subsequently they were used many times to calculate various flows [17,22].

No	Time, T	Length, L	Reference
1	const	const	—
2	$\min\left\{\frac{L_\mathrm{e}}{(2k/3)^{1/2}}, -\tau_\mathrm{p}\ln\left(1-\frac{L_\mathrm{e}}{\tau_\mathrm{p}\lvert\boldsymbol{v}-\boldsymbol{v}_\mathrm{p}\rvert}\right)\right\}$	L_e	[12]
3	$\left[\frac{(2k)^{1/2}}{2L_\mathrm{e}}+\frac{\lvert\boldsymbol{v}-\boldsymbol{v}_\mathrm{p}\rvert}{L_\mathrm{e}}\right]^{-1}$	—	[19]
4	$\min\{T_\mathrm{max}, T_\mathrm{c}\}$	L_e	[17,18]
5	$\frac{L_\mathrm{e}}{(2k/3)^{1/2}}$	—	[11]
6	$\frac{1}{T_\mathrm{L}}\exp\left(-T_\mathrm{e}/T_\mathrm{L}\right)$	—	[14]
7	$\min\left\{\frac{L_\mathrm{e}}{(2k/3)^{1/2}}, \frac{L_\mathrm{e}}{\lvert\boldsymbol{v}-\boldsymbol{v}_\mathrm{p}\rvert}\right\}$	—	[16]

Table 1: Different eddy lifetime models

In the model of [12], two time scales are introduced. As a time criterion, the minimum from the eddy lifetime and the time in which the particle passes through the eddy is used, and the spatial criterion is the integral scale of turbulence.

In the gravitational field, solid particles can scatter more intensively than liquid particles [8,18]. In the model of [18], the maximum particle and turbulent mole interaction time, T_max, which is independent of the solidliquid-particle interaction time, T_f, is introduced. The time T_max is determined on the basis of experimental data by the Lagrangian and Eulerian scales of turbulence related by the relation $T_\mathrm{L}=\beta T_\mathrm{E}$, where $\beta=v'T_\mathrm{e}/L_\mathrm{e}$. The criterion for the generation of a new fluid velocity is [18]

$$T=\begin{cases}\min\left(T_\mathrm{max},\, T_\mathrm{c}\right) & \text{if } 2L_\mathrm{e}>\tau_\mathrm{p}\left|\boldsymbol{v}-\boldsymbol{v}_\mathrm{p}\right|,\\ T_\mathrm{f}=2T_\mathrm{L} & \text{if } 2L_\mathrm{e}\leqslant\tau_\mathrm{p}\left|\boldsymbol{v}-\boldsymbol{v}_\mathrm{p}\right|.\end{cases}$$

The factor 2 takes into account the correction for experimental data. The model of [12] assumes that $T_\mathrm{max}=T_\mathrm{f}=T_\mathrm{e}$.

In anisotropy turbulent field, the eddy lifetime is given in the form [8,15]

$$T_{\mathrm{e}ij}\sim\left(\frac{k^2}{v_i'^2v_j'^2}\right)^{1/4}\frac{k}{\varepsilon}.$$

The velocity field is calculated on the basis of turbulence models for second moments. The model of [15] leads to an increase in computational costs with no marked increase in the accuracy of calculations [8].

In many models, the particle velocity is given as a superposition of the convective and diffusion components [7]. The first component is calculated on the basis of the deterministic approach, and the second one is assumed to be proportional to the concentration gradient of particles. The concentration is calculated from the diffusion equation. To the thus-found particle shift the random value chosen from the normal distribution in accordance with the turbulent diffusion coefficient of impurity is added. However, because of the difficulty of calculating effective particle transfer coefficients, such an approach has not found wide use.

Estimations show that for internal and jet flows the account of the criterion $T_{\max}$ introduced in [17, 18] has a weak effect on the particle dispersion, since the criterion for the generation of a new fluctuation of the fluid velocity is largely determined by the time $T_{\rm c}$. This conclusion is also confirmed by the calculations by the particle dispersion in the gravitational field [21].

The results of the calculations indicate that the realization of the stochastic model proves to be insensitive to the choice of the criterion for the generation of a new fluctuation of the fluid flow velocity. The conclusion drawn is corroborated by the results of [19], where criteria from 2 to 4 were compared.

Unlike the model of [12] in which the velocity fluctuation being calculated is assumed to be frozen inside the eddy during its lifetime, the present model considers that the particle is always under the action of the local turbulence at a point connected with its position. For this purpose, the fluctuations obtained at the start of the particle and eddy interaction are multiplied by the local turbulence intensity.

The disadvantage of the model is that the fluctuation fluid velocity field is not continuous, and the time dependence of the correlation coefficient is linear.

5 LANGEVIN-TYPE EQUATION

The Langevin-type equation is used to describe either only the fluid flow [33] or only the particle motion [34] or both of them [29].

5.1 Inertialess particle

To simulate the motion of an inertialess particle in a homogeneous isotropic turbulent field, the following stochastic equation is used [8]

$$d\boldsymbol{v} = \boldsymbol{v}(t+dt) - \boldsymbol{v}(t) = -\frac{\boldsymbol{v}}{T_{\rm L}}dt + \sigma\left(\frac{2}{T_{\rm L}}\right)^{1/2} d\boldsymbol{w}, \tag{5}$$

where dw is a Wiener random process (white noise), for which $\langle d\boldsymbol{w}\rangle = 0$, $\langle (d\boldsymbol{w})^2\rangle = dt$, $\langle dw_i(t) dw_j(t)\rangle = \delta_{ij} dt$. The velocity fluctuations are related to energy-containing eddies

with a time scale T_L. The velocity variance is obtained from the relation

$$\left\langle (d\boldsymbol{v})^2 \right\rangle = \left\langle [\boldsymbol{v}(t+dt) - \boldsymbol{v}(t)]^2 \right\rangle = \frac{2\sigma^2}{T_{\mathrm{L}}}\, dt.$$

In the inertial interval, the variance is a linear function of time, $\langle (d\boldsymbol{v})^2 \rangle = C_{\mathrm{K}} \varepsilon dt$. Therefore, $T_{\mathrm{L}} = 4k/(3C_{\mathrm{K}}\varepsilon) \sim k/\varepsilon$, which serves as a physical basis of the equation (5) used to simulate the diffusion of a fluid particle from a point source [33], the motion of inertialess particles in a turbulent flow [8, 34], and the passage to kinetic equations [31].

The multi-dimensional Markov's process, whose components satisfy the Langevin equation (5), can be compared to the Fokker–Planck equation for the probability density function. The solution of the latter shows that the mean-square particle displacement in the time interval dt is proportional to this interval $\langle (d\boldsymbol{r})^2 \rangle = 2Ddt$.

To take into account the turbulence inhomogeneity, additional terms are added to the equation (5) to provide a non-zero rms value of the random force (moments up to the sixth order are taken into account), and a mean pressure gradient is introduced. However, third- and higher-order moments play a secondary role compared to the second moments.

The model of [25] uses the assumption about the gradient character of the turbulent transfer, and the inertialess particle displacement is modelled on the basis of the equation

$$d\boldsymbol{r} = \frac{1}{\rho} \nabla \mu_t dt + \left(\frac{2\mu_t}{\rho} \right)^{1/2} d\boldsymbol{w}.$$

The turbulent viscosity is calculated by the Kolmogorov–Prandtl formula.

To take into account the correlation of velocities, the equation (5) is given in a modified form. In the case of homogeneous turbulence, the velocity at time t^{n+1} is related to the velocity at time t^n by the relation [32, 35]

$$v_i^{n+1} = R_{ii}(t,x) v_i^n + \sigma_i \left[1 - R_{ii}^2(t,x) \right]^{1/2} \xi_i(t). \tag{6}$$

In an inhomogeneous turbulent field, the equation (6) is written in the following form [30]

$$v_i^{n+1} = R_{ii}(t,x) v_i^n + \sigma_i \left[1 - R_{ii}^2(t,x) \right]^{1/2} \xi_i(t) + \left[1 - R_{ii}(t,x) \right] T_{\mathrm{L}ii} \frac{\partial \sigma_3}{\partial x_3} \delta_{i3}.$$

In the case of the step correlation function used in [24], the equation (6) takes the form

$$v_i^{n+1} = -\frac{\Delta t}{T_{\mathrm{L}ii}} v_i^n + \sigma_i \left[1 - \left(1 - \frac{\Delta t}{T_{\mathrm{L}ii}} \right)^2 \right]^{1/2} \xi_i(t).$$

The correlation function is a product of the Lagrangian and Eulerian correlations [39]

$$R_{ii}(t,x) = R_{\mathrm{L}ii}(t) R_{\mathrm{E}ii}(x).$$

In practice, various forms of the Lagrangian correlation function are used [39]

$$R_{\mathrm{L}ii}(t) = \exp\left[-\frac{t}{(q^2+1)T_{\mathrm{L}ii}}\right]\cos\left[\frac{q\,t}{(q^2+1)T_{\mathrm{L}ii}}\right], \quad R_{\mathrm{L}ii}(t) = \exp\left(-\frac{t}{T_{\mathrm{L}ii}}\right),$$

where $q > 0$. The Eulerian correlation function is usually expressed in terms of the longitudinal and transverse correlation coefficients based on von Karman relation [39]

$$R_{\mathrm{E}ij}(r) = [f(r) - g(r)]\,\frac{r_i r_j}{r^2} + g(r)\delta_{ij}.$$

These correlations coefficients for a homogeneous isotropic turbulence have the form

$$f(r) = \exp\left(-\frac{r}{L_{\mathrm{E}xx}}\right), \quad g(r) = \left(1 - \frac{r}{2L_{\mathrm{E}yy}}\right)\exp\left(-\frac{r}{L_{\mathrm{E}yy}}\right),$$

where $L_{\mathrm{E}xx} = 1.1T_{\mathrm{L}}\sigma$, $L_{\mathrm{E}yy} = 0.5L_{\mathrm{E}xx}$.

5.2 Inertial particle

In the model of [8], the random motion of a particle is modeled on the basis of the stochastic equation

$$d\boldsymbol{v}_{\mathrm{p}} = -\frac{\boldsymbol{v}_{\mathrm{p}}}{\tau_{\mathrm{p}}}dt + \sigma_{\mathrm{p}}\left(\frac{2}{\tau_{\mathrm{p}}}\right)^{1/2} d\boldsymbol{w},$$

which coincides formally with (5) but is characterized by different time scales. In a homogeneous isotropic turbulence, the velocity variance of the particle and fluid are related by the relation [39]

$$\frac{\sigma_{\mathrm{p}}^2}{\sigma^2} = \frac{1}{1 + \alpha\tau_{\mathrm{p}}/T_{\mathrm{L}}},$$

where $\alpha \sim 1.0$. For a homogeneous isotropic turbulence, $\sigma^2 = 2k/3$ and $T_{\mathrm{L}} = \beta k/\varepsilon$, where $\beta \sim 0.11 \div 0.60$. In the gravitational field, the relative motion of the particle and the fluid are taken into account [23].

In discrete form, the Langevin equation is written as

$$\boldsymbol{v}^{n+1} = a\boldsymbol{v}^n + b\boldsymbol{\xi}^n, \tag{7}$$

where $\boldsymbol{\xi}^n \in N(0,1)$. Multiplying relation (7) by $\boldsymbol{v}^n$, $\boldsymbol{v}^{n+1}$ and making averaging, we obtain

$$a = \frac{\langle \boldsymbol{v}^n \boldsymbol{v}^{n+1}\rangle}{\langle \boldsymbol{v}^n\rangle\langle \boldsymbol{v}^n\rangle} = R_{\mathrm{L}}(t), \quad b^2 = \left\langle \boldsymbol{v}^{n+1}\boldsymbol{v}^{n+1}\right\rangle - a^2\langle \boldsymbol{v}^n\rangle\langle \boldsymbol{v}^n\rangle = \sigma^2(1-a^2),$$

where $\sigma^2 = \langle(\boldsymbol{v}^n)^2\rangle$, $\boldsymbol{\xi}^n\sqrt{\Delta t} \to d\boldsymbol{w}$ at $\Delta t \to 0$, $\Delta t = t^{n+1} - t^n$. When the exponential correlation function is used, the coefficients acquire the following values

$$a = \exp\left(-\frac{\Delta t}{T_{\mathrm{L}}}\right), \quad b = \sigma\left(1 - a^2\right)^{1/2}.$$

At $\tau_p \to 0$ (light particles) the correlation function is Lagrangian, and at $\tau_p \to \infty$ (heavy particles) it is Eulerian.

5.3 Variants of Lagrangian models

Consider a solid particle P and a fluid particle F that coincide at the time t^n (Figure 2). Because of the inertia, their positions differ at the time t^{n+1}. To calculate the velocity of the fluid particle at the time t^{n+1}, either the one-step (Lagrangian) or the two-step (Lagrangian–Eulerian) approaches are used.

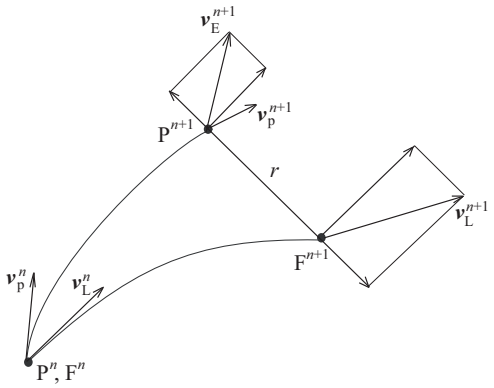

Figure 2: Fluid flow velocity at the times t^n and t^{n+1}

5.3.1 One-step approach

In the model of [15, 26], the fluid velocity at the time t^{n+1} is expressed in terms of the velocity of the same particle at the time t^n. The fluid velocity at the time t^{n+1} is

$$\boldsymbol{v}_{\mathrm{L}}^{n+1} = a\boldsymbol{v}_{\mathrm{L}}^{n} + b\boldsymbol{\xi}^{n}.$$

The coefficients a and b are described by the same relations as for the equation (7). Instead of the time scale T_L, the scale T_L^* is used. It is obtained with the aid of the linear interpolation between T_{L} and T_{E}

$$T_{\mathrm{L}}^* = \frac{\omega}{T_{\mathrm{L}}} + \frac{1-\omega}{T_{\mathrm{E}}},$$

where $\omega = \sigma_{\mathrm{p}}^2/\sigma^2$. From the above relation it follows that $T_{\mathrm{L}}^* \to T_{\mathrm{L}}$ at $\tau_{\mathrm{p}} \to 0$ and $T_{\mathrm{L}}^* \to T_{\mathrm{E}}$ at $\tau_{\mathrm{p}} \to \infty$. In [29], the time scale is calculated by the relation

$$T_{\mathrm{L}}^* = T_{\mathrm{L}} \left(1 + \frac{\beta C}{\sqrt{1 + T_{\mathrm{L}}/\tau_{\mathrm{p}}}} \right)^{-1},$$

where $C = 2\sqrt{2\pi}$, $\beta = T_{\mathrm{L}}/T_{\mathrm{E}}$. However, such an approach leads to incorrect limiting relations, in particular, at $\tau_{\mathrm{p}}/T_{\mathrm{L}} \gg 1$ (heavy particles) the time scale is

$$T_{\mathrm{L}}^* = \frac{T_{\mathrm{L}}}{1 + \beta C} = 0.4 T_{\mathrm{L}}.$$

5.3.2 Two-step approach

This approach consists of the Lagrangian step, where the fluid velocity at the time t^{n+1} is calculated from the velocity of the same particle at the time t^n, and the following Eulerian step. At the Eulerian step, the fluid velocity at the point where the solid particle is situated (Figure 1) is generated from the velocity at the time t^{n+1} of the fluid particle situated at distance r from the solid particle. The Lagrangian step is described by

$$\boldsymbol{v}_{\mathrm{L}}^{n+1} = a_{\mathrm{L}}\boldsymbol{v}_{\mathrm{L}}^{n} + b_{\mathrm{L}}\boldsymbol{\xi}_{\mathrm{L}}^{n}. \tag{8}$$

At the Eulerian step, the time variables are substituted into their spatial equivalents [27]

$$\boldsymbol{v}_{\mathrm{E}}^{n+1} = a_{\mathrm{E}}\boldsymbol{v}_{\mathrm{L}}^{n+1} + b_{\mathrm{E}}\boldsymbol{\xi}_{\mathrm{E}}^{n+1}. \tag{9}$$

Here, $\boldsymbol{\xi}_{\mathrm{L}}^{n} \in N(0,1)$, $\boldsymbol{\xi}_{\mathrm{E}}^{n+1} \in N(0,1)$. The coefficients a_L and b_L depend on the form of the Lagrangian correlation function, and the coefficients a_E and b_E are determined by the form of the Eulerian correlation function.

The distance between the fluid and the solid particles at the time t^{n+1} is expressed in terms of their instantaneous velocities $r = \left|\boldsymbol{v}^{n+1} - \boldsymbol{v}_{\mathrm{p}}^{n+1}\right| \Delta t$, where $\Delta t = t^{n+1} - t^{n}$. Because of the spatial correlation anisotropy, the calculated relations are written in the local coordinate system whose x-axis is directed from the fluid particle to the solid one.

For the Lagrangian step at $\Delta t \to 0$, the equation (8) goes over into the Langevin-type equation (5), which has heuristic basis [29]. For the Eulerian step, from (9) we obtain

$$d\boldsymbol{v} = -\frac{\boldsymbol{v}}{L_{\mathrm{E}}}dx + \sigma\left(\frac{2}{T_{\mathrm{E}}}\right)^{1/2} d\boldsymbol{w}. \tag{10}$$

The velocity difference at the distance r is $\Delta\boldsymbol{v} = \boldsymbol{v}(x+r) - \boldsymbol{v}(x)$. Taking into account that the velocity fluctuations obey the normal probability distribution, we obtain

$$\langle\Delta\boldsymbol{v}\rangle = 0, \quad \left\langle(\Delta\boldsymbol{v})^2\right\rangle = 2\sigma^2\frac{r}{L_{\mathrm{E}}}, \quad \left\langle(\Delta\boldsymbol{v})^3\right\rangle = 0.$$

On the other hand, the Kolmogorov's theory gives the following relations [39]

$$\langle\Delta\boldsymbol{v}\rangle = 0, \quad \left\langle(\Delta\boldsymbol{v})^2\right\rangle = (\varepsilon r)^{2/3}, \quad \left\langle(\Delta\boldsymbol{v})^3\right\rangle = \varepsilon r.$$

Consequently, the equation (10) contradicts the Kolmogorov law in the inertial range. Moreover, the equation (10) does not admit energy transfer from large eddies to small ones. Unlike the equation (8) used at the Lagrangian step, the equation (9), which describes the Eulerian step, has a less sound theoretical basis.

In the model of [26], a finite correlation length $\Lambda \sim L_{\mathrm{E}}$ was introduced. The position of the fluid and solid particles is tracked until the distance between them becomes equal Λ, since the velocities of two turbulent eddies at a distance larger than L_{E} are non-correlated. At $r > \Lambda$ we assume $R_{\mathrm{E}}(r) = 0$. At $r \leqslant \Lambda$ the exponential form of the Eulerian correlation function is used. This approach is not suitable for small particles [29].

5.3.3 Modified approach

In the model of [29], a modified representation of the Eulerian step described by relation (9) was introduced. The distance between the fluid and the solid particles is calculated by their mean relative velocity $r = \left|\langle \boldsymbol{v}^{n+1}\rangle - \langle \boldsymbol{v}_{\rm p}^{n+1}\rangle\right| \Delta t$. The velocities at the Lagrangian and Eulerian steps are determined by the following relations

$$\boldsymbol{v}_{\rm L}^{n+1} = a_{\rm L}\boldsymbol{v}^{n} + b_{\rm L}\boldsymbol{\xi}_{\rm L}^{n}, \quad \boldsymbol{v}_{\rm E}^{n+1} = a_{\rm E}\boldsymbol{v}_{\rm L}^{n+1} + b_{\rm E}\boldsymbol{\xi}_{\rm E}^{n+1}.$$

For exponential approximation of the Lagrangian and Eulerian correlations, we obtain

$$a_{\rm L} = \exp\left(-\frac{\Delta t}{T_{\rm L}}\right), \quad b_{\rm L} = \sigma\left(1 - a_{\rm L}^2\right)^{1/2}, \quad \boldsymbol{\xi}_L \in N(0,1);$$
$$a_{\rm E} = \exp\left(-\frac{\Delta t}{T_{\rm E}}\right), \quad b_{\rm E} = \sigma\left(1 - a_{\rm E}^2\right)^{1/2}, \quad \boldsymbol{\xi}_{\rm E} \in N(0,1).$$

The fluid velocity at the point where particle resides at the time t^{n+1} is calculated as

$$\boldsymbol{v}^{n+1} = a_1\boldsymbol{v}_{\rm L}^{n+1} + a_2\boldsymbol{v}_{\rm E}^{n+1} + b\boldsymbol{\xi}^{n+1}. \tag{11}$$

The coefficients a_1, a_2, and b in the equation (11) depend on the ratio $\sigma_{\rm p}/\sigma$ and the form of the time correlation function. For large particles, the point P^{n+1} is closer to the point F^n, and for small particles it is closer to F^{n+1}. Particles of medium sizes are positioned between the points F^n and F^{n+1} (Figure 3).

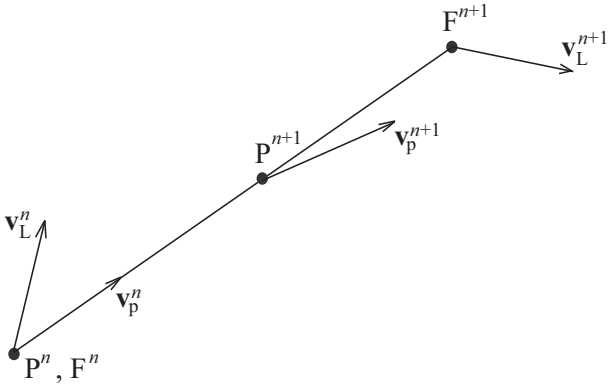

Figure 3: Position of the solid particle relative to the fluid particle at the time t^n and t^{n+1}

Unlike the models of [30,32,35], where $\Delta t \sim 0.2T_{\rm L}$, the time integration step is chosen from the condition $\Delta t = \alpha \min\{\Delta t_1, \Delta t_2, \Delta t_3\}$, where Δt_1 is the time required for the particle to cross the control volume of the Eulerian mesh, $\Delta t_2 = T_{\rm L}$, $\Delta t_3 = \tau_{\rm p}$, $\alpha \sim 0.5$.

6 NUMERICAL METHOD

The CFD solver works in an explicit time-marching fashion, based on a three-step Runge–Kutta stepping procedure. The fluxes are divided into the inviscid and viscous components. The central difference scheme of the 2nd order is used for viscous fluxes, and piecewise parabolic method and Chakravarthy–Osher scheme are used for inviscid fluxes [40]. Convergence to a steady state is accelerated by the use of multi-grid techniques, and by the application of Jacobi preconditioning.

To solve the Cauchy problem for particle equations, the fourth-order Runge–Kutta method and methods that permit resolving in the solution rapidly and slowly decaying components are used. To supply fluid parameters at points lying in the particle trajectory, the bilinear interpolation method is employed. The integration step along each trajectory was limited to the time and space turbulence scales. In the calculations, from 1000 to 10,000 trajectories of sample particles depending on their size were modeled.

7 RESULTS

The width and length of channel are $h = 0.01$ m and $L = 0.6$ m. The mesh contains $400 \times 100 \times 50$ nodes, and is refined in x and y directions. Minimal and maximum mesh steps are $\Delta x_{\min} = 1.5 \times 10^{-5}$ m, $\Delta x_{\max} = 1.2 \times 10^{-4}$ m, $\Delta y_{\min} = 1.8 \times 10^{-5}$ m, $\Delta y_{\max} = 2 \times 10^{-4}$ m. The mesh is uniform in z direction, $\Delta z = 10^{-4}$ m. Time steep is $\Delta t = 2.5 \times 10^{-6}$ s, and 50,000 time steps are performed.

At high Reynolds numbers ($\mathrm{Re} \sim 10^3$), the flow region in the channel with wall injection is divided into sub-region of singulary influence of viscosity near the walls and sub-region of vortical flow in the core. Viscous forces play negligible role compared to inertial forces at all x except for small region near the left wall at $x/h < 12$. The maximum of streamwise velocity comes towards the solid wall of the channel, near which the zone of viscous flow in the likeness of boundary layer on a flat plate is developed (Figure 4a, one-sided injection). With increase in distance from left end of the channel, the profile of streamwise velocity takes a more filled shape than a profile computed from the k–ε model. The solution is independent on Reynolds number at two-sided injection. The profiles of streamwise velocity are more filled than before compared to those based on the model of vortical flow of incompressible fluid in the channel with wall injection or k–ε turbulence model (Figure 4b, two-sided injectioon). Profiles of transverse velocity demonstrates a weak dependency on the injection velocity in the wide interval of parameters of the problem.

Distribution of streamwise velocity along x coordinate is close to linear dependence (Figure 5a). The profiles of transverse velocity have universal behavior, and depend on x coordinate weakly. Starting from $x/h \sim 30$, the profiles of transverse velocity become independent on x coordinate. The results based on k–ε model show divergence of distribution of streamwise velocity from linear dependence at $x/h > 35$ [9].

Laminar–turbulent transition is defined by the distribution of friction coefficient along solid wall of the channel (see Figure 5b). The results computed show that the k–ε model

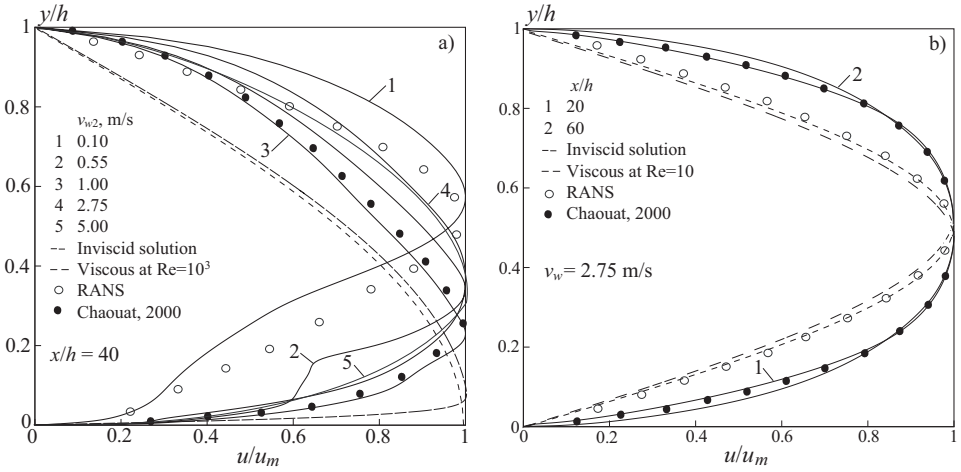

Figure 4: Profiles of streamwise velocity

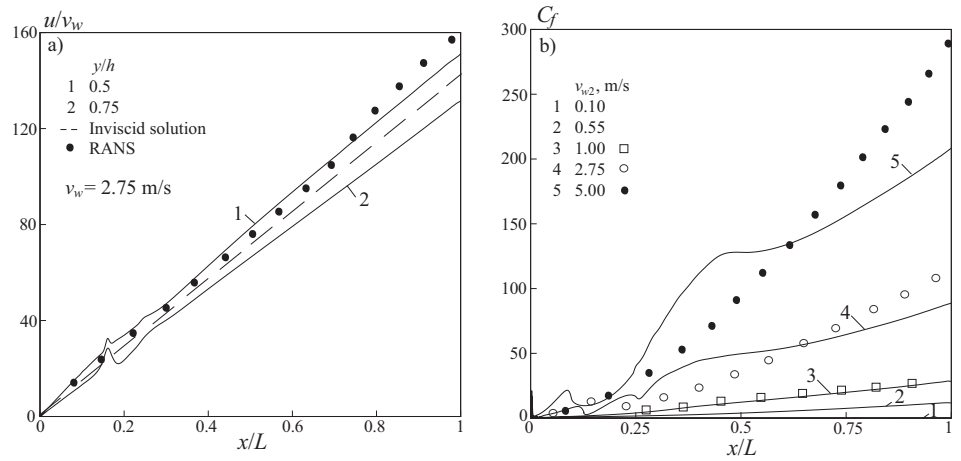

Figure 5: Distributions of streamwise velocity and friction coefficient

gives satisfactory prediction of friction coefficient at small injection velocities (line 3). The discrepancy of the results based on LES and k–ε model increases moving from left boundary of the channel. Increase in friction coefficient, starting with $x/L \sim 0.2$, corresponds to the laminar–turbulent transition. Location of transition point depends on parameters of the problem, and is sensible to fluctuations of velocity on a wall. The transition point is moved downstream with increase in the injection velocity. Coordinate of the transition point agrees with the data of [4]. The flow pattern computed allows marking the following flow regimes: (i) region with considerable influence of viscous forces ($x/h < 1/\mathrm{Re}$), (ii) region of laminar flow with cosine profile of streamwise velocity (1¡$x/h < 5$), (iii) transition region ($5 < x/h <$10–15), (iv) region of turbulent flow (10–15$< x/h$). The length of laminar flow depends on Reynolds number. The coordinate of transition point decreases with increasing relative amplitude of perturbations at $k_m^{1/2}/u_m > 4\%$.

The results of [9] based on k–ε model predict maximum of turbulent kinetic energy far from the permeable wall of the channel and overpredict a turbulence intensity near the walls compared to experimental data and results of DNS presented in [3, 4].

A specific feature of the flow in a channel with injection is the presence of a negative pressure gradient, which strongly influences the mechanism and intensity of turbulent transfer. An increase in the level of turbulent velocity fluctuations is observed in the region of a strong shear at a distance from the permeable wall of the channel where the fluid particles moving normally to the surface have to turn around in the narrow near-surface zone. The results of the calculations are in fair agreement with the data of the physical experiment of [3], excepting the wall-adjacent zones of the flow where the calculation gives a higher turbulence intensity [4].

Figure 6 presents the trajectories of aluminum oxide particles (r_p = 5–50 μm) in a channel with two-sided injection (v_w = 5 m/sec, $u_{p,w} = 0$ and $v_{p,w} = v_w$). The influence of the sluggishness of a particle on its scattering is inconclusive, since particles of different masses execute motion in different regions with a different turbulence intensity. The influence of velocity fluctuations on the particle motion is manifest when the particle gets into the turbulent region of the flow. A nonmonotonic change in the turbulent kinetic energy along the axial coordinate leads to a nonmonotonic change in the degree of particle involvement in the fluid flow, which is determined by the relation between the particle relaxation time and the turbulent time scale.

The particle time-averaged trajectories and profile of particle concentration are presented in the Figure 7. The results of calculation of the motion and scattering of aluminum oxide particles (r_p = 5–10 μm) for various particle sizes (Stokes numbers) are shown in the Figure 8. At the initial instant of time the particle was on the upper wall of the channel. The calculations were made beginning from the point $x_{p0} = 3$ with a step $\Delta x = 3$. The calculation was finished when the particle either left the calculated region (at $x/h > 30$) or fell onto the lower wall of the channel (at $y = 0$).

For particles of large fractions (r_p = 30-50 μm), velocity fluctuations produce no significant effect on the impurity motion throughout the region of flow development because of the inertia of such particles (Figure 8a, b). Weak migration of particles towards decreasing turbulent kinetic energy is observed only for particles injected into the channel at a considerable distance from its left end (at $x_{p0} > 9$). Small particles (r_p = 5-15 μm) are scattered rather strongly (Figure 8c, d).

The correlation function of small particles practically follows the distribution obtained for the carrier flow (small particles are involved in the pulsation motion of the carrier flow and move along the streamlines), and are well described by the exponential dependence often postulated in calculations (Figure 9). The correlation coefficient of large particles differs in quality from the distribution that takes place for the carrier flow (large particles deviate from the streamlines, largely manifesting their inertia). The transverse correlation coefficient therewith acquires small negative values.

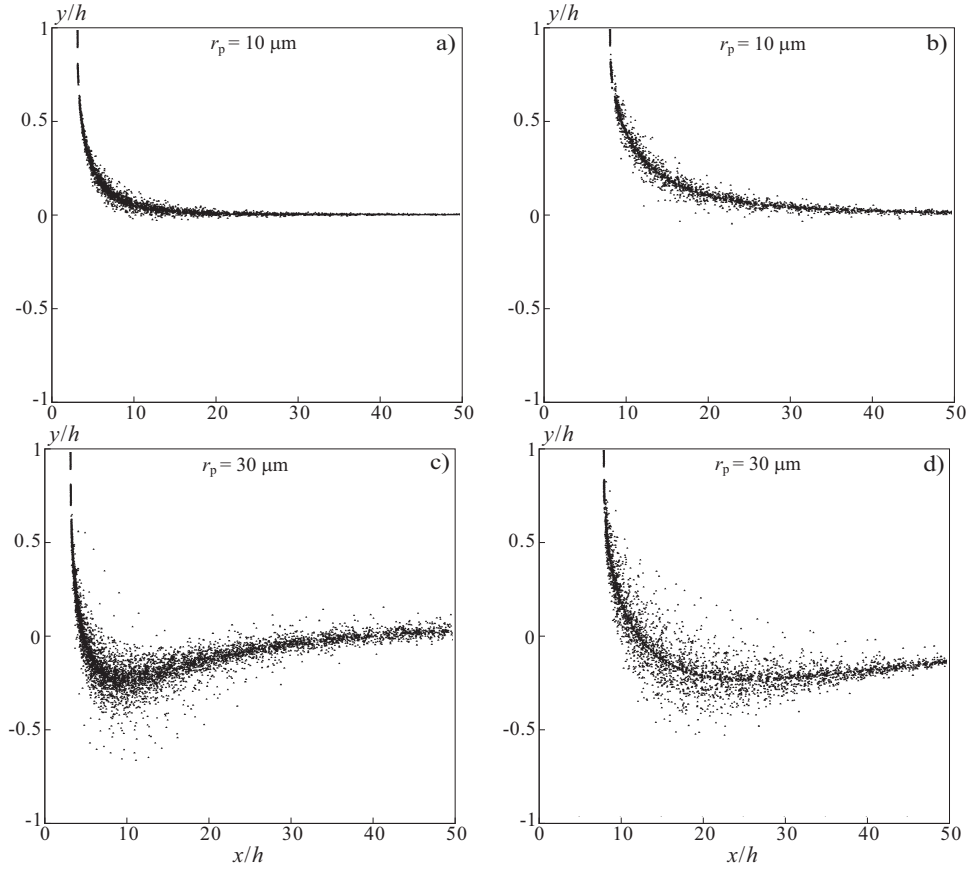

Figure 6: Trajectories of sample particles in the channel at $v_w = 5$ m/s

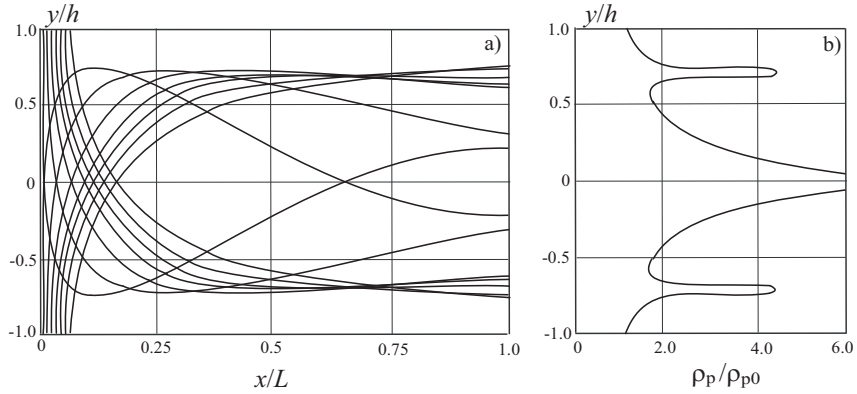

Figure 7: Particle trajectories and profile of particle concentration

8 CONCLUSION

The features of the formulation and realization of various stochastic models of motion and scattering of condensed impurity particles in a turbulent flow have been considered.

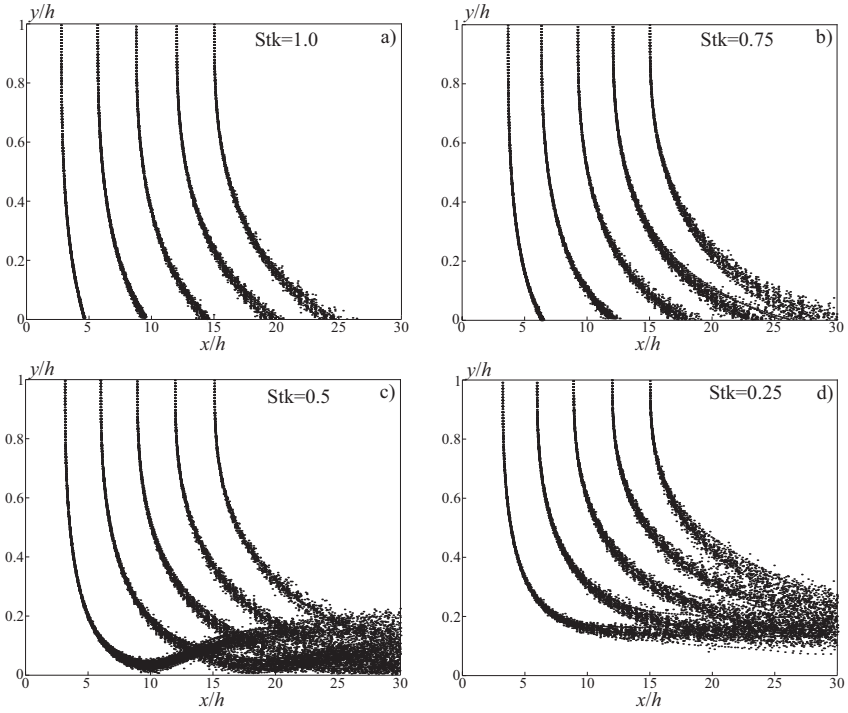

Figure 8: Particle trajectories in the channel

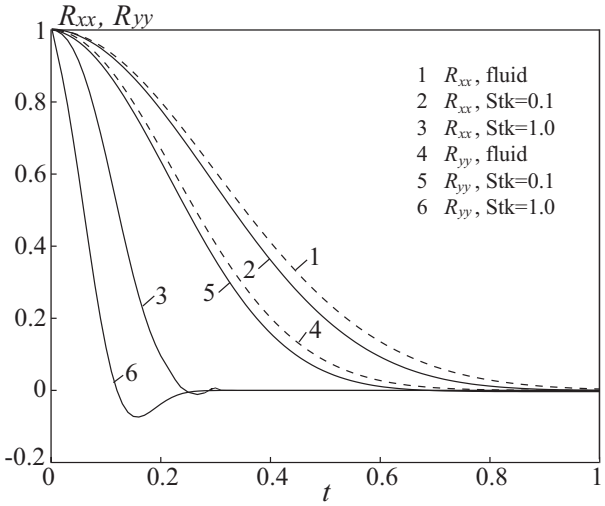

Figure 9: Correlation functions of fluid and particles

The possibilities of the stochastic approach based on the integration of a Langevin-type equation have been demonstrated with the example of the calculation of the turbulent flow of a gas suspension in a channel with injection for various values of the injection rate and the sizes of particles and conditions of their introduction into the channel. The results

obtained on its basis show that velocity fluctuations of the carrier turbulent flow strongly influence the motion and scattering of dispersive impurity, and the proposed model leads to satisfactory results that agree with the data of numerical and physical experiments.

The application of the method of simulation of large vortices for describing the velocity field of the carrier turbulent flow makes it possible to upgrade the universality of the method, as well as to avoid the application of semi-empirical relations for calculating the statistical characteristics of turbulence and the assumption of local inhomogeneity and isotropy of the turbulence field.

REFERENCES

[1] F. Vuillot and N. Lupoglazoff, Combustion and turbulent flow effects in 2D unsteady Navier–Stokes simulations of oscillatory solid rocket motors, *AIAA Paper* 96-0884 (1996).

[2] A. Ciucci, G. Iaccarino, R. Moser, F. Najjar and P. Durbin, Simulation of rocket motor internal flows with turbulent mass injection, *Center for Turbulence Research, Stanford University*, 245–266 (1998).

[3] B. Chaouat, Numerical simulation of channel flows with fluid injection using Reynolds stress model, *AIAA Paper* 2000-0992 (2000).

[4] A. Kourta, Instability of channel flow with fluid injection and partial vortex shedding, *Computers and Fluids*, **33**(2), 155–178 (2004).

[5] K.N. Volkov, Large-eddy simulation of turbulent gas-particle flows in the duct induced by the wall injection, *Computational Fluid and Solid Mechanics*, Elsevier Science Ltd, Amsterdam, 928–931 (2005).

[6] K. Volkov, Large-eddy simulation of free shear and wall-bounded turbulent flows, *Atmospheric Turbulence, Meteorological Modeling and Aerodynamics*, Nova Science, USA (2010).

[7] C.T. Crowe, T.R. Troutt and J.N. Chung, Numerical models for two-phase turbulent flows, *Annual Review of Fluid Mechanics*, **28**, 11–43 (1996).

[8] D. Lakehal, On the modelling of multiphase turbulent flows for environmental and hydrodynamic applications, *International Journal of Multiphase Flow*, **28**(5), 823–863 (2002).

[9] K.N. Volkov, Stochastic modelling of impurity motion and scattering in the mechanics of turbulent gas-dispersed flows, *Journal of Engineering Physics and Thermophysics*, **77**(5), 883–894 (2004).

[10] K. Volkov, Stochastic models of particle motion in a turbulent flow and their application for calculating internal flows, *Journal of Engineering Physics and Thermophysics*, **80**(3), 570–582 (2007).

[11] J.K. Dukowicz, A particle-fluid numerical model for liquid sprays, *Journal of Computational Physics*, **35**(2), 229–253 (1980).

[12] A.D. Gosman and E. Ioannides, Aspects of computer simulation of liquid-fueled combustors, *AIAA Paper* 81-0323 (1981).

[13] J.S. Sabnis, S.-K. Choi, R.C. Buggeln and H.J. Gibeling, Computation of two-phase shear-layer flow using an Eulerian–Lagrangian analysis, *AIAA Paper* 88-3202 (1988).

[14] M. Sommerfeld and G. Zivkovic, Recent advances in the numerical simulation of pneumatic conveying through systems, *Computational Methods in Applied Sciences*, Elsevier Science Ltd, Amsterdam, 201–212 (1992).

[15] D. Burry and G. Bergeles, Dispersion of particles in anisotropic turbulent flows, *International Journal of Multiphase Flow*, **19**(4), 651–664 (1993).

[16] J.F. Chauvot, L. Dumas and K. Schmeisser, Modelling of alumina slag formation in solid rocket motors, *AIAA Paper* 95-2728 (1995).

[17] D.I. Graham and P.W. James, Turbulent dispersion of particles using eddy interaction models, *International Journal of Multiphase Flow*, **22**(1), 157–175 (1996).

[18] D.I. Graham, Improved eddy interaction models with random length and times scales, *International Journal of Multiphase Flow*, **24**(2), 335–345 (1998).

[19] N. Cesco, L. Dumas, T. Pevergne and Y. Fabignon, Stochastic models to the investigation of slag accumulation in a large solid rocket motors, *AIAA Paper* 97-2785 (1997).

[20] Y. Wang and P.W. James, On the effect of anisotropy on the turbulent dispersion and deposition of small particles, *International Journal of Multiphase Flow*, **25**(3), 551–558 (1999).

[21] X.-Q. Chen, Heavy particle dispersion in inhomogeneous, anisotropic turbulent flows, *International Journal of Multiphase Flow*, **26**(4), 635–661 (2000).

[22] E.A. Matida, K. Nishino and K. Torii, Statistical simulation of particle deposition on the wall from turbulent dispersed pipe flow, *International Journal of Heat and Fluid Flow*, **21**(4), 389–402 (2000).

[23] G.T. Csanady, Turbulent diffusion of heavy particles in the atmosphere, *Journal of the Atmospheric Sciences*, **20**(3), 201–208 (1963).

[24] P.A. Durbin, A random flight model of inhomogeneous turbulent dispersion, *Physics of Fluids*, **23**(11), 2151–2153 (1980).

[25] S.B. Pope, PDE methods for turbulent reactive flows, *Progress in Energy and Combustion Science*, **11**, 119–192 (1985).

[26] A. Berlemont, Desjonqueres, and G. Gouesbet, Particle Lagrangian simulation in turbulent flows, *International Journal of Multiphase Flow*, **16**(1), 19–34 (1990).

[27] Q. Zhou and M.A. Leschziner, A time-correlated stochastic model for particle dispersion in anisotropic turbulence, In proceedings of the *8th Symposium on Turbulent Shear Flows*, Munich, Germany, 10.3.1–10.3.6 (1991).

[28] A.M. Reynolds, A Lagrangian stochastic model for particle trajectories in non-Gaussian turbulent flows, *Fluid Dynamics Research*, **19**, 277–288 (1997).

[29] J. Pozorski and J.-P. Minier, On the Lagrangian turbulent dispersion models based on the Langevin equation, *International Journal of Multiphase Flow*, **24**(6), 913–945 (1998).

[30] J. Lataste, D. Huilier and H. Burnage, Influence of the fluid turbulence on the dispersion of heavy particles in a turbulent boundary layer, *Academy of Sciences of Paris*, **327**(8), 731–738 (1999).

[31] J.-P. Minier and E. Peirano, The PDF approach to turbulent polydispersed two-phase flows, *Physics Report*, **352**, 1–214 (2001).

[32] M. Sommerfeld, Validation of a stochastic Lagrangian modeling approach for interparticle collisions in homogeneous isotropic turbulence, *International Journal of Multiphase Flow*, **27**(11), 1829–1858 (2001).

[33] Y. Mito and T.J. Hanratty, Lagrangian stochastic simulation of turbulent dispersion of heat markers in a channel flow, *International Journal of Heat and Mass Transfer*, **46**(6), 1063–1073 (2003).

[34] R. Rzehak and W. Zimmermann, Inertial effects in Brownian motion of a trapped particle in shear flow, *Physica A*, **324**, 495–508 (2003).

[35] D. Huilier, On the necessity of including the turbulence experienced by an inertial particle in Lagrangian random-walk models, *Mechanics Research Communications*, **31**, 237–242 (2004).

[36] A. Yakhot, S.A. Orszag, V. Yakhot and M. Israeli, Renormalization group formulation of large-eddy simulation, *Journal of Scientific Computing*, **1**(1), 1-51 (1986).

[37] J. Smagorinsky, General circulation experiments with the primitive equations, *Monthly Weather Review*, **91**(3), 99–165 (1963).

[38] S. Shen, F. Ding, J. Han, Y.-L. Lin, S.P. Arya and F.H. Proctor, Numerical modeling studies of wake vortices: real case simulation, *AIAA Paper* 99-0755 (1999).

[39] J.O. Hinze, Turbulence, McGraw Hill (1975).

[40] S.R. Chakravarthy and S. Osher, A new class of high-accuracy TVD schemes for hyperbolic conservation laws, *AIAA Paper* 85-0363 (1985).